Square-well fluids in confined space with discretely attractive wall-fluid potentials: Critical point shift

Xianren Zhang* and Wenchuan Wang
Division of Molecular and Materials Simulation, Key Lab for Nanomaterials, Ministry of Education, Beijing University of Chemical Technology, Beijing 100029, China

(Received 9 May 2006; revised manuscript received 9 October 2006; published 18 December 2006)

In this work the effects of the wall-fluid interaction on the critical point shift are studied by using a discrete and attractive wall-fluid interaction and density functional theory. In contrast to the previous assumption, it is found that the dependence of critical temperature shift on the wall-fluid interaction does not simply show a monotonic manner, but increases with the strength of the interaction for weak surfaces, then decreases for strong surfaces. The similar trend holds for the systems with different fluid-fluid interactions and different confined spaces. Unlike the capillary critical temperature, the critical density of square-well fluids in a confined space increases monotonically as the wall-fluid interaction becomes more attractive.

DOI: 10.1103/PhysRevE.74.062601 PACS number(s): 68.43.−h, 68.35.Rh, 61.46.Fg, 61.30.Hn

The capillary critical temperature of a confined fluid is found to be lower than that of the bulk by experiments, theory, and computer simulations [1–15]. The interesting surface-driven critical point shift is induced, on the one hand, by the finite size effect, and on the other hand, by the introduction of the wall force. The dependences of critical temperature shift on the pore size were well studied [2–5,8,11], whereas systematic investigations of the effects of the wall-fluid interaction, to our knowledge, are quite rare. It is partly attributed to the fact that for a continuous wall-fluid potential model, the finite size and wall force effects could not be separated from each other. The dependence of the critical temperature shift of fluids in a confined space on the wall-fluid interaction is generally believed to be monotonic [3], based on the scaling theory prediction and mean field theory. Vishnyakov *et al.* [11] also compared two different wall-fluid interactions and found that the critical temperatures in narrow pores for the stronger adsorption field will be lower than the weaker one. Brovchenko *et al.* [12] studied phase behaviors of water molecules in slit and cylindrical pores and found that the critical temperature in the pores with weak and moderate strength of wall-water interaction decrease with the increase of the strength of wall-water interaction.

The aim of this study is to check the previous assumption by Fisher and Nakanishi [3] and to find out the dependence of the critical temperature shift of confined fluids on the wall-fluid interaction. Similar to our previous work [16], a discrete wall-fluid potential model and density functional theory (DFT) were used in this work. The artificial and square well-like wall-fluid potential combines two attractive square-well potentials, of which the deeper potential (namely, deep well) near the surface of the cylindrical pore approximates the potential minimum of a realistic potential function, and the shallower describes its long tail. The main advantage of this model is that it provides a way to completely separate the finite size effects and the influence of wall-fluid interaction. The discrete wall-fluid potential $(\sigma_{\text{tail}}, \sigma_{\text{tail}}+\sigma_{\text{dw}}, \varepsilon_{\text{tail}}, \varepsilon_{\text{dw}})$ is described by four parameters, as described in our previous work [16], in which ε_{dw} and $\varepsilon_{\text{tail}}$ denote the depths of the deep well potential and the tail potential, while σ_{dw} and σ_{tail} represent their widths, respectively [see Fig. 1(a)]. Here, σ_{dw} is set to 0.5, and $\varepsilon_{\text{tail}}$ is set to 0 for simplicity. Hence, a wall-fluid potential in this work can be given by $(R-0.5, R, 0, \varepsilon_{\text{dw}})$, where $R=\sigma_{\text{dw}}+\sigma_{\text{tail}}$ is the pore radius. The discrete wall-fluid potential in fact turns out to be a square-well (SW) potential. In this work, the fluid-fluid interaction is also modeled by a SW potential [see Fig. 1(b)], and its interaction range and strength are defined by λ and ε, respectively. DFT is used in this work to investigate the coexistence region and critical point shift of pure SW fluids in confined spaces. The choice of the DFT was dictated by reasons of computational efficiency. Similar results could, in principle, be obtained through computer simulations. However, the computational cost is not affordable for the study of wall-fluid interaction dependence of critical point shift. The DFT applied here is the version proposed by Tarazona [17,18]. The details for the DFT calculation can be referred to in our previous paper [16]. Appropriate reduced

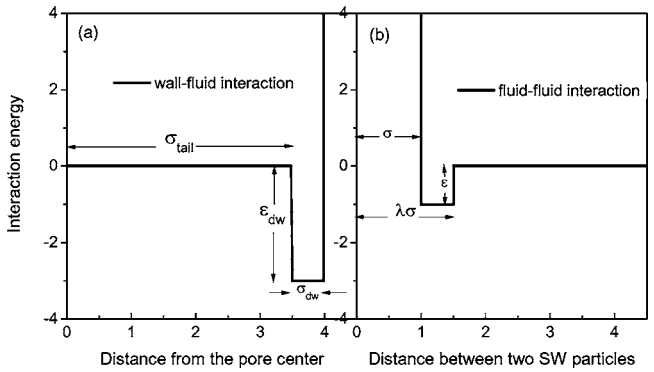

FIG. 1. A schematic diagram of the wall-fluid interaction and the fluid-fluid interaction. (a) For the wall-fluid interaction, ε_{dw} denotes the depths of the deep-well potential, and σ_{dw} and σ_{tail} represent the widths of the deep-well potential and the tail potential, respectively. (b) For the fluid-fluid interaction, σ is the particle diameter, while λ and ε are the interaction range and strength parameters, respectively.

*Electronic mail: zhangxr@mail.buct.edu.cn

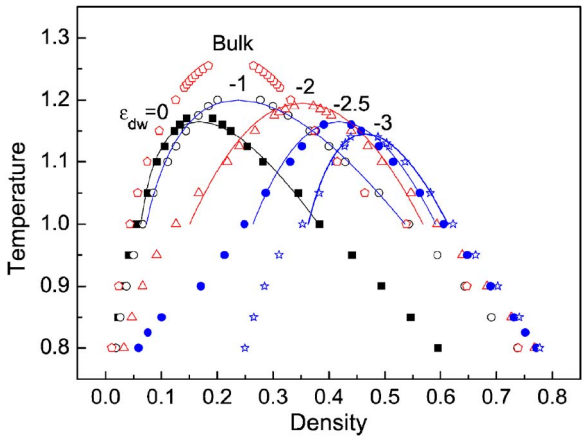

FIG. 2. (Color online) Phase diagram of the confined square-well fluid with $\lambda=1.5$ at different wall-fluid interactions, $\varepsilon_{dw}=0, -1, -2, -2.5, -3$. Solid lines represent a nonlinear regression fitting to the data by using Eq. (1). The left and right branches of the envelopes represent the densities of the gaslike phase and the liquidlike phase in pores at equilibrium, respectively.

quantities (temperature T^* and density ρ^*) can be defined by scaling with respect to the energy parameter ε and the particle diameter σ, e.g., $T^*=k_BT/\varepsilon$ and $\rho^*=\rho\sigma^3$, where k_B is the Boltzmann constant. In the remainder of this paper, we omit asterisks from reduced quantities for simplicity.

Before studying the critical point shift of confined SW fluid, the bulk coexistence curves were calculated by DFT for comparison. As an approximation, we computed the bulk coexistence curve using DFT method for confined system, while the radius of a cylindrical pore is set to 16σ and $\varepsilon_{dw}=0$. Although 16σ is chosen here somewhat artificially, it is large enough to neglect the effects of porous walls. It is noted that when the temperature is approaching the capillary critical temperature of the fluid in a pore, the distance between the liquidlike and gaslike branches of the phase envelope increasingly decreases, which makes it more difficult to locate the capillary condensation. For this reason, in these runs the ranges of chemical potentials explored in DFT calculations were carefully tuned until the transitions were included and the equilibrium states were determined by the grand potential in enough precision [16].

We gradually decreased the parameter ε_{dw} from a hard wall (a purely repulsive wall with $\varepsilon_{dw}=0$) to a much more attractive wall for the effects of the wall-fluid interaction. Our results for the temperature-density coexistence curves for the SW fluids of $\lambda=1.5$ in cylindrical pores with different wall-fluid interactions are given in Fig. 2, together with the bulk coexistence curve for comparison. Generally, when the wall-fluid interactions become more attractive, the coexistence densities for both the liquidlike and vaporlike branches move to the higher values. It is interesting to find in Fig. 2 that for the systems with weak wall-fluid interactions, the liquidlike branches of the coexistence curves move faster than the gaslike branches, thus widening the phase envelopes, as the strength of the attractive wall-fluid interaction increases. In contrast, for strongly attractive wall-fluid interactions, the vaporlike branches of the coexistence curves move faster, and the phase envelopes hence become narrow with the increase of the strength of the wall-fluid interaction. Consequently, the confined system with the widest coexistence curve is neither the case with the weakest wall-fluid interaction, $\varepsilon_{dw}=0$, nor the case with the strongest wall-fluid attractive interaction, $\varepsilon_{dw}=-3$, but the case of $\varepsilon_{dw}=-1$ instead (see Fig. 2). Consideration of the variation of the shape and width of the critical region with the wall-fluid interaction would lead us to check the assumption of the wall-fluid interaction dependence of critical temperature shift [3]. Here, we determined the critical point properties of the SW fluids in confined spaces through our DFT data by following the procedure of Vega *et al.* [19], using a nonlinear regression

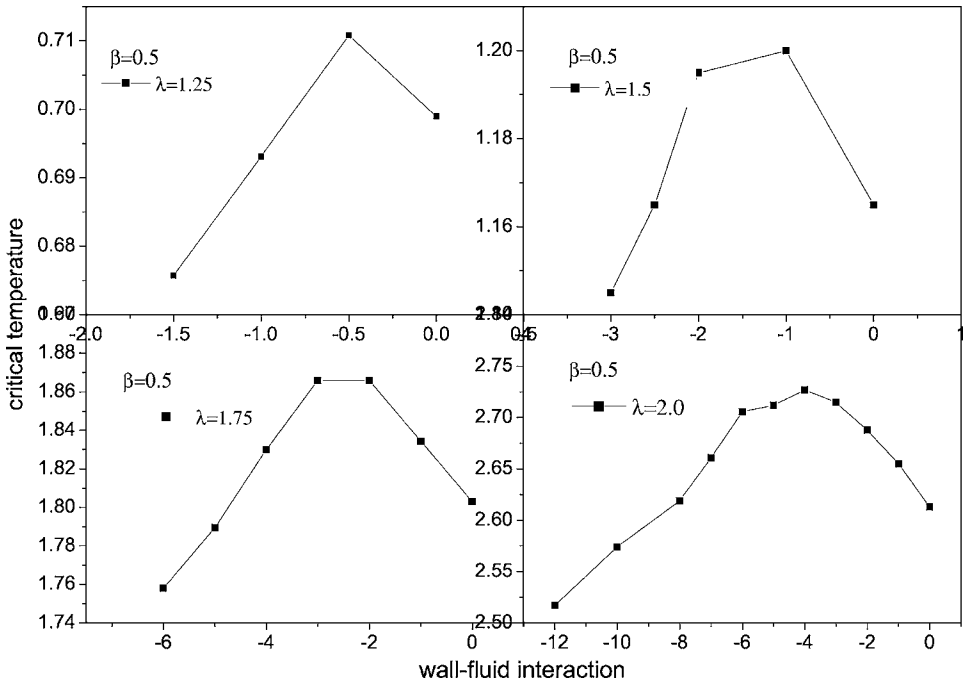

FIG. 3. The effect of wall-fluid interaction on capillary critical temperature of the square-well fluids with different λ values, $\lambda=1.25$, 1.5, 1.75, and 2.0, in a pore of radius 4σ.

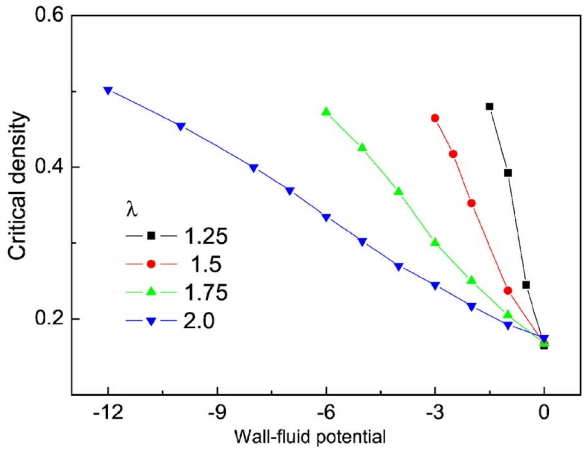

FIG. 4. (Color online) The critical density changing with the wall-fluid interaction for square-well fluids with different λ values in a pore of radius 4σ.

procedure to fit the coexistence densities to the expression

$$\rho_{\pm} = \rho_c + A(T_c - T) \pm 0.5B(T_c - T)^{\beta}, \quad (1)$$

where + is for liquid phase and − is for vapor phase. The equation is also used to get the capillary critical point of confined fluid in literature [11,14,15,19,20]. The critical exponent β is set to 0.5 in this work, and the amplitudes A and B are treated as adjustable parameters in order to achieve the best fit of the calculated data.

Figure 3 shows the effects of the wall-fluid interaction on the capillary critical temperature, in which four SW fluids with λ=1.25, 1.5, 1.75, and 2.0 are considered. It is strikingly found that the critical temperature does not increase with the wall-fluid interaction simply in a monotonic way. In contrast, it increases first with the strength of the interaction for weak surfaces, then decreases for strong surfaces. For instance, the capillary critical temperature of the fluid of λ =1.5 increases from 1.17 to 1.2 as the wall-fluid interaction decreases from the hard wall, i.e., $\varepsilon_{dw}=0$ to −1, then decreases when the attractive interaction decreases further. Moreover, the location of the maximum critical temperature depends on the interaction range of the SW fluid λ, as is shown in Fig. 3. The increase of the interaction range of SW will lead to more pronounced changes of the location of the maxima from the hard wall. For example, the maximum of the capillary critical temperature for SW fluid λ=1.25 is located at $\varepsilon_{dw}=-0.5$, while its location moves to −1 for λ=1.5, −2 for λ=1.75, and −4 for λ=2.0, respectively.

The critical density of a confined fluid also depends on the wall-fluid and fluid-fluid interactions, which are shown in Fig. 4. Unlike the capillary critical temperature, the critical density of an SW fluid in a confined space increases monotonically as the wall-fluid interaction becomes more attractive, which is consistent with the coexistence densities we mentioned above (see Fig. 2). Just like the behavior of bulk Lennard-Jones and SW fluids [17], the critical densities for different SW fluids in the pores with zero wall-fluid interaction are nearly the same within the range of uncertainty, regardless of the range of the attractive interaction, λ. But, the critical densities would depend on λ if the wall-fluid interaction is not zero. Within the range of the wall-fluid interaction we studied, the fluid-fluid interaction of the shorter range would result in a higher critical density, as is shown in Fig. 4.

Now, we turn to the reason for the nonmonotonic behavior of the coexistence curve, and hence the nonmonotonic behavior of the critical temperature shift, as a function of the wall-fluid interaction. Two density profiles, corresponding to the states before and after the capillary condensation from the adsorption branch, respectively, are shown in Fig. 5(a), in which the SW fluid of λ=1.5 is confined in a cylindrical pore of 4σ with a wall-fluid interaction $\varepsilon_{dw}=0$. As a comparison, the local structures for $\varepsilon_{dw}=-1$ and −3 are also shown in Figs. 5(b) and 5(c), respectively. Examination of the density profiles of Figs. 5(a)–5(c) reveals that there are three qualitatively distinct adsorption behaviors as the wall-fluid inter-

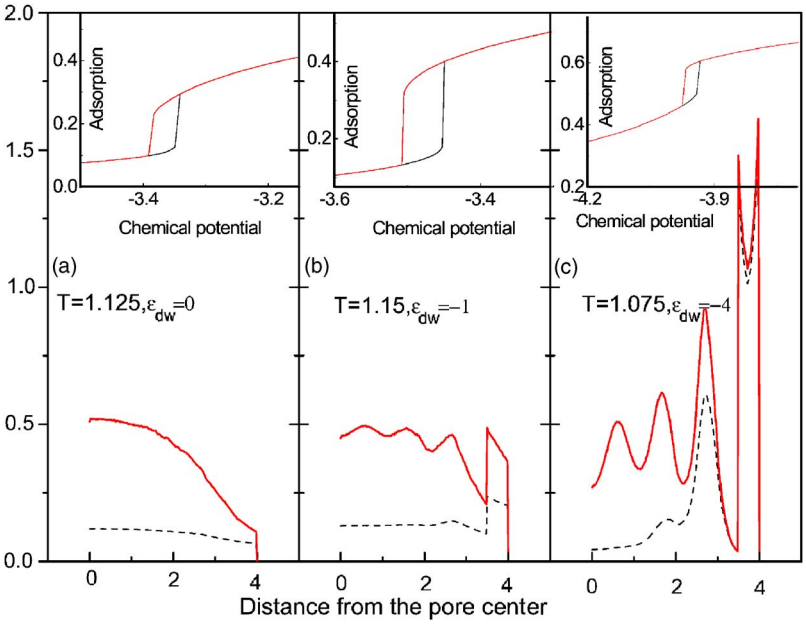

FIG. 5. (Color online) Two density profiles for the SW fluid of λ=1.5 at temperature $T/T_{cc}\approx 0.96$, corresponding to the states before and after the capillary condensation from the adsorption branch, respectively, for the different wall-fluid potential. (a) $\varepsilon_{dw}=0$ and the two curves correspond to two chemical potentials of $\mu=-3.42$ and −3.33, respectively. (b) $\varepsilon_{dw}=-1$ and the two curves correspond to the two chemical potentials of $\mu=-3.475$ and −3.472, respectively. (c) $\varepsilon_{dw}=-3$ and the two curves correspond to the two chemical potentials of $\mu=-3.91$ and −3.83, respectively. The insets show the corresponding adsorption isotherms.

action varies. For the system with the weakest wall-fluid interaction, i.e., the purely repulsive interaction of a hard wall, the density profiles in Fig. 5(a) show a strong density depletion near the wall, which appears as a gradual density decay due to the presence of the wall. This agrees with the depletion of the liquid water density near hydrophobic surfaces detected by computer simulation [13]. In the case of the moderately stronger wall-fluid interaction, for example, $\varepsilon_{dw}=-1$ shown in Fig. 5(b), the profiles show a fully developed adsorbed layer near the wall in the liquidlike phase because of the attractive wall-fluid interaction, while the adsorption is weak enough so that the layer can be largely removed in the gaslike phase. This is why the confined fluids with moderate wall-fluid interactions are of the widest binodal curves, and thus why the capillary critical temperature presents a maximum in this range of the wall-fluid interaction (see Fig. 3). As the strength of the wall-fluid interaction increases further, the adsorbed layer shows a pronounced peak and the molecules in the layer are nearly fixed in the critical region, as is the case for $\varepsilon_{dw}=-3$ in Fig. 5(c), which is equivalent to reducing the effective pore radius from 4 to 3.5 or less, as is argued by Fisher and Nakanishi [2,3]. This is why the capillary critical temperature decreases as the wall-fluid interaction becomes more attractive.

We also studied the dependence of critical temperature on pore size for the SW fluid of $\lambda=1.5$. For large pore sizes (data are not shown), such as $R=6\sigma$ and 8σ, the trend of critical temperatures behaves similarly compared with that of pore 4σ, i.e., the T_{cc} increases with the strength of the wall-fluid interaction for the weak surfaces, then decreases for the strong attractive surfaces. It is also found that the decrease of pore size enhances the critical temperature shift, being consistent with the literature [3–5].

In summary, in this work we investigated the influence of the wall-fluid interaction on the critical point shift by DFT calculations. In contrast to the previous assumption, it is strikingly found that the dependence of the critical temperature shift on the wall-fluid interaction does not take a monotonic manner, but increases with the strength of the interaction for weak surfaces, then decreases for strong surfaces. The similar trend is found for the systems with different fluid-fluid interactions and for the systems with different confined spaces. In addition, it is found that not only the capillary critical temperature but also the critical density of confined fluids depends on the strength of the wall-fluid interaction. Unlike the capillary critical temperature, the critical density of SW fluids in a confined space increases monotonically, as the wall-fluid interaction becomes more attractive.

We thank Wei Dong (ENS-Lyon, France) for stimulating discussions. This work was supported by National Scientific Foundation of China (Grant No. 20236010) and by "Chemical Grid Project" of Beijing University of Chemical Technology. X.Z. acknowledges the support of the Research Foundation for Young Researchers of BUCT.

[1] L. D. Gelb, K. E. Gubbins, R. Radhakrishnan, and M. Sliwinska-Bartkowiak, Rep. Prog. Phys. **62**, 1573 (1999).
[2] M. E. Fisher and H. Nakanishi, J. Chem. Phys. **75**, 5857 (1981).
[3] H. Nakanishi and M. E. Fisher, J. Chem. Phys. **78**, 3279 (1983).
[4] R. Evans, U. Marini Bertollo Marconi, and P. Tarazona, J. Chem. Phys. **84**, 2376 (1986).
[5] A. de Kreizer, T. Michalski, and G. H. Findenegg, Pure Appl. Chem. **63**, 1495 (1991).
[6] B. K. Peterson, K. E. Gubbins, G. S. Heffelfinger, U. M. B. Marconi, and F. van Swol, J. Chem. Phys. **88**, 6487 (1988).
[7] G. S. Heffelfinger, Z. Tan, K. E. Gubbins, U. M. B. Marconi, and F. van Swol, Mol. Simul. **2**, 393 (1989).
[8] A. Z. Panagiotopoulos, Mol. Phys. **62**, 701 (1987).
[9] S. Y. Jiang, C. L. Rhykerd, and K. E. Gubbins, Mol. Phys. **79**, 373 (1993).
[10] J. Forsman and C. E. Woodward, Mol. Phys. **96**, 189 (1999).
[11] A. Vishnyakov, E. M. Piotrovskaya, E. N. Brodskaya, E. V. Votyakov, and Yu. K. Tovbin, Langmuir **17**, 4451 (2001).
[12] I. Brovchenko, A. Geiger, and A. Oleinikova, J. Chem. Phys. **120**, 1958 (2004).
[13] I. Brovchenko, A. Geiger, and A. Oleinikova, J. Phys.: Condens. Matter **16**, S5345 (2004).
[14] J. Jiang, S. I. Sandler, and B. Smit, Nano Lett. **4**, 241 (2004).
[15] A. V. Neimark and A. Vishnyakov, J. Phys. Chem. B **110**, 9403 (2006).
[16] X. Zhang, D. Cao, and W. Wang, J. Chem. Phys. **119**, 12586 (2003).
[17] P. Tarazona, Phys. Rev. A **31**, 2672 (1985); **32**, 3148(E) (1985).
[18] P. Tarazona, U. Marini Bettolo Marconi, and R. Evans, Mol. Phys. **60**, 573 (1987).
[19] L. Vega, E. de Miguel, L. F. Rull, G. Jackson, and I. A. McLure, J. Chem. Phys. **96**, 2296 (1992).
[20] H. L. Vortler and W. R. Smith, J. Chem. Phys. **112**, 5168 (2003).